European Conference on Computational Fluid Dynamics
ECCOMAS CFD 2006
P. Wesseling, E. Oñate and J. Périaux (Eds)

ON 3D NUMERICAL SIMULATIONS OF VISCOELASTIC FLUIDS

D.Niedziela, O.Iliev and A.Latz

Fraunhofer Institute for Industrial Mathematics,
Fraunhofer-Platz 1, D-67663, Germany.
e-mail: {niedziel,iliev,latz}@itwm.fhg.de
web page: www.itwm.fhg.de

Key words: non–Newtonian fluids, anisotropic viscosity, integral constitutive equation

Abstract. *In this work we present and solve a class of non–Newtonian viscoelastic fluid flow problems. Models for non-Newtonian fluids can be classified into three large groups depending on the type of the constitutive relation used: algebraic, differential and integral. The first type of models are most simple one, the last are the most physically adequate ones. Here we consider some models from the first and the third groups, and present robust and efficient algorithms for their solution. We present new mathematical model, which belongs to the class of generalized Newtonian models and is able to account for the anisotropy of the viscosity tensor observed in many real liquids. In particular, we discuss a unified model that captures both shear thinning and extensional thickening for complex flows. The resulting large variations of the viscosity tensor in space and time are leading to a strong numerical coupling of the momentum equations due to the appearance of mixed derivatives in the discretization. To treat this strong coupling appropriately, we present two modifications of classical projection methods (like e.g. SIMPLE). In the first modification all momentum equations are solved coupled (i.e. mixed derivative are discretized implicitly) but still iterations are performed between the momentum equations and the continuity equation. The second one is a fully coupled method, where momentum and continuity equation are solved together using a proper preconditioner. The models involving integral constitutive relation which accounts for the history of deformations, result in a system of integro-differential equations. To solve it, we suggest a proper splitting scheme, which treats the integral and the differential parts consecutively. Integral Oldroyd B and Doi Edwards models are used to simulate flows of dilute and concentrated polymer solutions, respectively.*

1 INTRODUCTION

Newtonian liquids are defined by a linear constitutive relation between the strain- and stress tensor with a scalar and constant viscosity as proportionality factor. In Non-Newtonian liquids this linear relation is not valid anymore. The form of the constitutive

relations become material dependent and the dynamics e.g. the strain rate field, temperature and pressure can enter in a much more complicated way. As long as the microscopic dynamics of the liquid does not interfere with the hydrodynamic time scale the stress strain relation can still be assumed to be local in time i.e the stress only depends on the current values of the strain rate tensor and other dynamic quantities. But if the relation between stress tensor and strain rate tensor becomes nonlinear the local isotropy of the liquid is very likely to be violated. In fact the most general relation between stress tensor ($\boldsymbol{\sigma}$) and strain rate tensor ($\boldsymbol{\gamma}$), which is still local in time is given by

$$\sigma_{i,j} = \eta_{ij,lm}(\boldsymbol{\gamma})\gamma_{l,m} \tag{1}$$

Locally axially symmetric liquids in which the axis of symmetry is given by local flow velocity are considered in this paper. For such liquids the simple Newtonian relation between stress and strain tensor is generalized to

$$\sigma_{ij} = \eta(\dot{\gamma})(\gamma_{ij} - \gamma_{ii}\delta_{ij}) + \eta_e(\dot{\epsilon})\gamma_{ii}\delta_{ij} \tag{2}$$

where η_e and η are extensional and shear viscosities, respectively, depending on the local averaged shear rate $\dot{\gamma}$ and the local extension rate $\dot{\epsilon}$ to be introduced below. Fluids, which show decrease of shear viscosity upon increase of shear rate $\dot{\gamma}$ are called shear thinning. If the viscosity increases they are called shear thickening. In analogy liquids with decreasing or increasing extensional viscosity with increase of extensional strain rate $\dot{\epsilon}$ are called extensional- (tension-) thinning or thickening, respectively.

The most common model for pure shear thinning liquids is the Carreau model [17], or variants of it [9]. All of them are isotropic and therefore inconsistent in the sense that dependence of the viscosity on shear rate implies by definition, that the property of the liquid should depend on the direction of shearing.

Viscoelastic fluids, however, consist of both short and long relaxation modes, and therefore such local stress–strain relation is not valid anymore. In order to calculate stress tensor at certain particle position, one has to take the full history of the deformations of this particle into account, not only the one which can be determined from current stress. In such case, the stress tensor can be written in general integral constitutive equation formulation as

$$\boldsymbol{\sigma} = \int_{-\infty}^{t} \mu(t,t') f_t(t'),$$

where $\mu(t,t')$ is the memory function and $f_t(t')$ is a model dependent nonlinear strain measure relative to the current time t. In this paper for simulations of dilute polymer solutions we use integral Oldroyd B model [15, 17] and for concentrated ones integral Doi Edwards model [7].

For all models describing generalized Newtonian fluids variations of viscosity results in strong coupling of the momentum equations through their viscous term. Additionally, the momentum equations are coupled through the convective term and the pressure. Due

to varying viscosities, one has to take into account discretization of the mixed derivatives appearing in the momentum equations. In many commercial solvers those terms are treated in explicit way, i.e. calculated from the corresponding values computed in the previous time step and taken as a source term. This may lead to the restriction on the time step used in simulations due to the stability problems. To avoid it, here the momentum equations are discretized and treated in coupled manner, i.e. the mixed derivatives are discretized in implicit way. We also present here two solution techniques used in simulations of generalized Newtonian fluids, that improve their stability properties, namely coupled momentum projection method (which is extension of classical projection methods, like SIMPLE) and fully coupled method. In the latter continuity and momentum equations are solved simultaneously.

The paper is organized as follows. In Section 2 we present the system of governing equations that are used in simulations. Next, in Section 3, we describe in more details solution techniques used in calculations. Further, we present numerical results (Section 4). First, validation with shear–thinning fluids modeled by Carreau viscosity model is given. Then, we show results from simulations of anisotropic viscosity fluids described by the model proposed in this paper. Further, simulation results of polymer solutions described by integral type constitutive equations are shown. Finally, we discuss performance of different solution techniques used in simulations of generalized Newtonian fluids.

2 GOVERNING EQUATIONS

The flow of incompressible and isothermal non–Newtonian fluids are governed by continuity and momentum equations

$$\nabla \cdot \mathbf{v} = 0, \tag{3}$$

$$\rho \frac{\partial \mathbf{v}}{\partial t} + (\rho \mathbf{v} \cdot \nabla)\mathbf{v} = -\nabla p + \nabla \cdot \boldsymbol{\sigma}, \tag{4}$$

where $\mathbf{v}$ stands for velocity, p denotes pressure, ρ denotes density and $\boldsymbol{\sigma}$ stands for stress tensor. In order to close the above system of equations, the latter has to be describe by a constitutive equation.

2.1 Algebraic constitutive equations

In the class of generalized Newtonian fluids, the stress tensor is related with rate of deformation tensor $\boldsymbol{\gamma} = (\nabla \mathbf{v} + \nabla^T \mathbf{v})$ by some algebraic formula. Let us first describe isotropic viscosity model used in this paper. From many isotropic viscosity models, that are reviewed in [17], we choose a very common one, namely Carreau model. Its viscosity is expressed as

$$\eta(\dot{\gamma}) = \eta_0 (1 + (Cu\dot{\gamma})^2)^{\frac{(n-1)}{2}}, \tag{5}$$

where shear–rate is defined by $\dot{\gamma} = \sqrt{\frac{1}{2}\sum_{ij} \gamma_{ij}\gamma_{ji}}$, η_0 is the zero shear–rate viscosity and Cu, n are the parameters to fit experimental data. With the above defined viscosity, the

stress tensor $\boldsymbol{\sigma}$ takes the following form

$$\boldsymbol{\sigma} = \eta(\dot{\gamma})\boldsymbol{\gamma}. \tag{6}$$

This model has showed a good ability in capturing shear–viscosity properties and is still widely used in commercial softwares.

Over many years isotropic models like Carreau, that can capture shear behavior of fluids were extensively studied. However, up to the knowledge of the authors there is still a lack of simple algebraic models being able to deal with the combined effect of shear–thinning (thickening) and extensional–thickening (thinning). Simple means, that it should have similar structure as the Carreau model, thus could be considered as its natural extension. Moreover, this model should be easily applicable for an arbitrary flow domains. Therefore, such model is proposed in this paper. Let us first define extensional strain rate as

$$\dot{\epsilon} = \vec{t} \cdot \boldsymbol{\gamma}\vec{t}, \tag{7}$$

where $\vec{t}$ is given by

$$\vec{t} = \frac{\mathbf{v}}{\|\mathbf{v}\|} \tag{8}$$

and denotes unit vector parallel to the flow direction. The same definition may be found in [14], where authors discuss how to perform the measurements of elongational viscosity. Now, having defined extensional strain rate $\dot{\epsilon}$, one can also use Carreau model to describe extensional viscosity behavior as

$$\eta_e(\dot{\epsilon}) = \eta_0(1 + (Cu_e\dot{\epsilon})^2)^{\frac{(n_e-1)}{2}} \tag{9}$$

with fitting parameters n_e, Cu_e. Next step in modeling is to define the constitutive equation, which should include both, shear $\eta(\dot{\gamma})$ and extensional $\eta_e(\dot{\epsilon})$ viscosities. Therefore, taking into account the fact, that the diagonal terms of rate of strain tensor γ_{ii} represent the rate of elongation of an element of the fluid in respective $i-$ direction, whilst the off-diagonal terms $\gamma_{ij}(i \neq j)$ express deformations of a fluid element (what corresponds to shearing), the stress tensor will now be defined as

$$\sigma_{ij} = \eta(\dot{\gamma})(\gamma_{ij} - \delta_{ij}\gamma_{ii}) + \eta_e(\dot{\epsilon})\delta_{ij}\gamma_{ii}. \tag{10}$$

Note, that the shear viscosity η enters the off–diagonal terms of the stress, while the extensional viscosity η_e only the diagonal ones. This simple model includes both shear and extensional effects, modeled by $\eta(\dot{\gamma})$ and $\eta_e(\dot{\epsilon})$ respectively. Therefore, it allows simulations of shear–thinning and extensional–thickening fluids, for example. Moreover, it is very easy to add to (5, 9) the viscosity dependence from pressure and temperature, what may result, for example, in a kind of Cross–WLF model.

2.2 Integral constitutive equations

Many natural and synthetic fluids are viscoelastic materials, for which the stress of a fluid particle depends not only on the current flow field, as for Newtonian or generalized Newtonian fluids, but also on the history of the deformation experienced by that particle, which can be specified by an integral models. In such case, the stress tensor $\boldsymbol{\sigma}$ is written in a following form

$$\boldsymbol{\sigma} = \eta_0 \boldsymbol{\gamma} + \mathbf{T}, \tag{11}$$

where $\eta_0 \boldsymbol{\gamma}$ is Newtonian and $\mathbf{T}$ is elastic parts of the stress tensor. In this work we apply our numerical algorithm to two different integral models, the Oldroyd B and the Doi - Edwards model within the independent alignment approximation. The Oldroyd B model has a differential form and an equivalent integral form [15]. In the integral formulation the polymeric stress is expressed as

$$\mathbf{T} = \frac{\eta_p}{\lambda^2} \int_{-\infty}^{t} dt' \mu(t,t') \mathbf{B}(t,t'), \tag{12}$$

where λ is the relaxation time, and η_p quantifies the amount of coupling between deformations of the polymer and the flow.

$$\mu(t,t') = exp\left(-\frac{(t-t')}{\lambda}\right) \tag{13}$$

is again the memory function, and finally

$$\mathbf{B}(t,t') = \mathbf{E}(t,t') \cdot \mathbf{E}^T(t,t') \tag{14}$$

is the Finger strain tensor. The differential form of the Oldroyd B can be found e.g. in [17]. The polymeric stress contribution of the Doi - Edwards model [7] has a similar form as the Oldroyd B but a more complicated form for the effective strain produced by the conformations of the polymers.

$$\mathbf{T} = G_e \int_{-\infty}^{t} dt' \mu(t,t') \mathbf{Q}(t,t') \tag{15}$$

where G_e is the elastic modulus of the entanglement configuration of the polymers and

$$\mu(t,t') = \frac{1}{\tau_d} exp\left(-\frac{(t-t')}{\tau_d}\right) \tag{16}$$

is the memory function that weights the contributions of past deformations which influences the current stress. τ_d is as usual the effective tube relaxation time. We use different notation for relaxation times simply to be consistent with cited literature. The orientation tensor $\mathbf{Q}$ takes within the independent alignment approximation the form

$$\mathbf{Q}(t,t') = \left\langle \frac{(\mathbf{E}(t,t')\mathbf{u}(t')) \otimes (\mathbf{E}(t,t')\mathbf{u}(t'))}{\parallel \mathbf{E}(t,t')\mathbf{u}(t') \parallel} \right\rangle_0 \frac{1}{\langle \parallel \mathbf{E}(t,t')\mathbf{u}(t') \parallel \rangle_0}, \tag{17}$$

where $\mathbf{u}$ are unit vectors representing the orientation of a tube segment, $\otimes$ stands for the dyadic product and $\mathbf{E}(t,t')$ is the deformation tensor. The evolution equation for the deformation tensor appearing in (14,17) is given by [17]

$$\frac{D\mathbf{E}(t,t')}{Dt} = \left(\nabla \mathbf{v}(t)\right)^T \mathbf{E}(t,t') \tag{18}$$

with the initial condition

$$\mathbf{E}(t',t') = \mathbf{I}, \tag{19}$$

where $\mathbf{I}$ stands for identity matrix. The time derivative on the left-hand side in (18) is the material derivative, because we consider the deformation of a fluid particle while following the particle along its trajectory.

3 SOLUTION TECHNIQUES

The governing equations (3, 4) are discretized with use of finite volume method on collocated grid. The details of the space discretization are not discussed here, interested readers are referred to [10]. Here we concentrate on different approaches for time discretization.

3.1 Time splitting for system of integro–differential equations

To simulate the flows of viscoelastic fluids, modeled by the integral–type constitutive equation one has to solve a strongly coupled system of integro-differential equations. A decoupling approach, based on fractional time step discretization is used here. However, work on more advanced coupling and decoupling approaches is a part of future research. Shortly, the numerical algorithm reads as follows:

Step 1. Solve the continuity (3) and the momentum (4) equations taking the polymeric tensor $\mathbf{T}$ in (4) as a source term (i.e., from the previous time step calculation).

Step 2. Solve all the equations involved with integral constitutive equation (12, 15) using the velocity values obtained at *Step 1.*

Projection type, for example SIMPLE-like (see, e.g., [8]), or coupled algorithms are applied for solving the balance equations at Step 1. In fact, the current algorithm and software are extension of [10], where solution of the Newtonian flow problems are considered. The more interesting part of the algorithm is the non-Newtonian part, i.e. Step 2. To calculate extra stress tensor of the integral–type (12, 15) Deformation Field Method (DFM) is used at this point of our algorithm. For detailed description of this method interested reader is referred to [18, 19].

3.2 Iterative methods for varying viscosity problems

Let us now discuss solution techniques used in the generalized Newtonian flow problems. Suppose for a moment, that the continuity (3) and the momentum (4) equations are discretized in space. Denote by B^T the discretization of the gradient operator, B the discretization of the divergence operator, D_v the discretization of the diffusion (viscous) operator and C_v the discretization of the convection operator. We use superscript $^{n+1}$ to denote values at the new time level and superscript ^{n} to denote the old time values, $\tau = t^{n+1} - t^n$ stands for the time step. With such notations, the system of equations (3, 4), that has to be solved at each time step $t = t^{n+1}$, may be written in a matrix form as

$$\begin{pmatrix} A & B^T \\ B & 0 \end{pmatrix} \begin{pmatrix} \mathbf{v} \\ p \end{pmatrix} = \begin{pmatrix} f \\ 0 \end{pmatrix}, \tag{20}$$

where $f = \frac{\varrho \mathbf{v}^n}{\tau}$, $A = (\frac{\varrho}{\tau} I + C_v - D_v)$ and I stands for identity operator. Let us first discuss projection type methods. Instead of solving simultaneously the velocity an pressure components, the coupled problem (20) is divided into simpler equations of the Poisson and the convection-diffusion type. Projection–type methods, using the formalism of Turek [21], can be written as follows. First, momentum equations (4) are solved using pressure field known from the previous time iteration, what can be written as

$$\mathbf{v}^* = A^{-1}(f - B^T p^i). \tag{21}$$

Then, one solves pressure correction equation, derived with use of the continuity equation (3), i.e.

$$M \delta p^i = -B\mathbf{v}^*, \tag{22}$$

where $\mathbf{v}^*$ denotes solution of equation (21) for given p^i. M should be spectrally close to $BA^{-1}B^T$ and the usual choice of it is

$$M = BH^{-1}B^T, \tag{23}$$

where H is a diagonal matrix. Many possible choices were proposed, like $H = diag\{A\}$, which results in well known SIMPLE scheme. Modifications, like $H = diag(part\{A\})$, give different versions of the original SIMPLE algorithm (fractional time step projection method). After solving equation (22) new pressure field is calculated through its correction δp^i, i.e. $p^{i+1} = p^i + \delta p^i$. However, velocity $\mathbf{v}^*$ will not in general satisfy incompressibility constraint. Therefore, some correction has to be introduced to project it out on divergence free space. It is realized by taking

$$\mathbf{v}^{i+1} = \mathbf{v}^* + H^{-1}B^T \delta p^i. \tag{24}$$

Note, that contrary to Newtonian fluids, due to the varying viscosity in generalized Newtonian ones, matrix A has a full block representation of the form (2D description for simplicity)

$$A = \begin{pmatrix} A_{11} & A_{12} \\ A_{21} & A_{22} \end{pmatrix}, \tag{25}$$

where off–diagonal blocks $A_{ij}, i \neq j$ correspond to mixed derivatives appearing in momentum equations (4). In many commercial solvers they are discretized in explicit way and taken as a source term. However, space dependent viscosities bring additional coupling of the governing equations. Now, in addition to the coupling of the continuity (3) with the momentum (4) equations, and the coupling of the latter through the convective term, equations (4) are strongly coupled through their viscous term. Modification of the standard projection type methods, like SIMPLE, is done at point (21). The momentum equations are solved coupled, i.e. mixed derivatives are treated in implicit way. It is preferable for us due to stability reasons in simulations of the generalized Newtonian fluids with varying viscosity.

An alternative approach to the segregated solvers is the fully coupled solvers, where system (20) is solved at once. To speed up calculations, it is supplemented with a proper preconditioning technique. In general (see [5]) applying a preconditioned iterative method for solving a system of equations is equivalent to applying a non–preconditioned method for solving the transformed system. Several preconditioners for (20) are carefully analyzed in [4]. In [9], another approach is used, where different preconditioners are applied to first transformed system (20). In simulations presented here, we have used such approach, however for detailed description the interested reader is referred to [9].

4 NUMERICAL RESULTS

There is much interest in understanding the flow of viscoelastic fluids. Different effects, like shear and elongational rate dependent viscosities, elasticity of the fluid, etc., influence the flow. We study these effects individually, in order to better understand each of them.

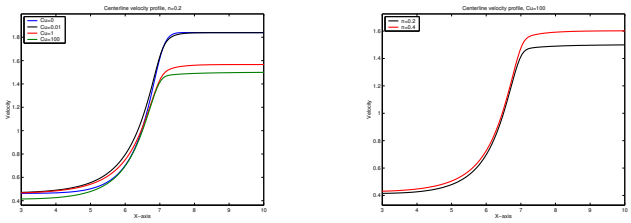

Figure 1: The effect of varying Cu number on the calculated centerline velocity for n=0.2, Carreau model (left plot). The effect of varying n number on the calculated centerline velocity for Cu=100, Carreau model (right plot).

4.1 Varying viscosity models

To investigate the interaction of shear-thinning, similarly as in [12], the Carreau model parameters Cu and n will be varied. The result will be discussed in terms of the centerline velocity profile and the upstream vortex size. As a test geometry we use 4:1 planar contraction domain. To exclude the inertial effects we choose the flow with Reynolds

number $Re = 10^{-2}$ defined as $Re = \frac{\rho \bar{U} L}{\eta_0}$, where $\rho = 1[\frac{g}{cm^3}]$ stands for fluid density, L is the width of the upstream channel, $\eta_0 = 100[Pas]$ is a zero–shear viscosity and $\bar{U}$ is average upstream channel velocity. Note, that for shear–thinning fluids local Reynolds numbers can be higher, especially near to the walls where higher shear–rates occur and decrease local viscosities even couple of order of magnitude. First, we examine the changes of the centerline velocity profiles for high shear–thinning fluid ($n = 0.2$) when changing Cu number. Results are presented in left plot of Figure 1. For $Cu = 0.01$ the axial velocity attain almost the same maximum as in Newtonian case ($Cu = 0$). This should be expected, since for such low Carreau number the shear–rate required for an onset of shear–thinning is almost not present. Carreau fluid, however, exhibits less steep axial velocity profile compared with the Newtonian one. Further increase of Carreau Cu number results in decrease of centerline velocity profiles. At $Cu = 100$, the flow is dominated by the power-law region of the viscosity function, and further increase of Cu number does not change the velocity profile. Next, decrease of power-law index n at constant Cu has quantitatively the same effect as increasing Cu at constant n. It is shown in right plot of Figure 1. The reason for such behavior is that both combinations lead to more shear–thinning. Another well known fact is that shear–thinning decreases the sizes of the upstream vortices compared to the Newtonian fluids of the same zero–shear rate viscosity. The more shear–thinning the fluid is, the smaller vortices it exhibits [12]. The effect of shear thinning can be weakened by increase of extensional stress. This was shown in an experimental study of polymer melts [23, 24]. Although in this paper the origin of the increasing extensional stress is the increasing elasticity of the investigated fluid and thus different from the mechanisms captured in our model, similar arguments apply. In both cases vortex growth is caused by increasing extensional stresses in the entry region.

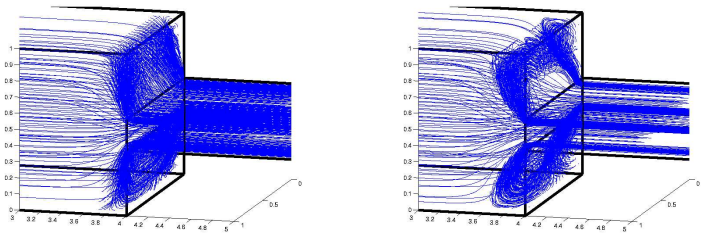

Figure 2: 3D planar contraction geometry. Streamline plots, Newtonian fluid (left figure) and extensional–thickening fluid (right figure).

Vortices are formed as a stress relief mechanism. Only materials with an extensional viscosity that increases with extensional rate exhibit vortex enhancement, whereas no, or only small, vortices are present for the materials where extensional viscosity decreases or remains constant with elongational rate. To validate the performance of the model (10) and being able to distinguish between shear and extensional properties of the fluid, we choose shear–thinning and extensional–thickening liquid with the fluid parameters: $Cu = 1, n = 0.8, Cu_e = 1, n_e = 2$ and zero-shear viscosity $\eta_0 = 10[Pas]$. As a test

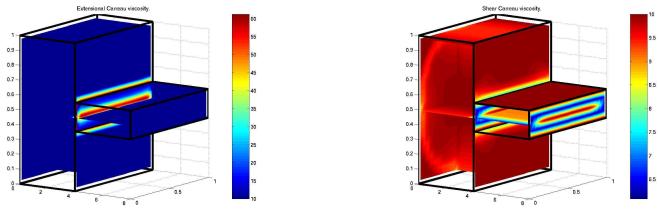

Figure 3: 3D planar contraction geometry. Extensional viscosity (left figure) and shear viscosity (right figure).

geometries, we choose after Evans and Walters [13] 7:1 planar contraction and 7:1 square–to–square contraction domains. As it was discussed, shear–thinning itself decreases the vortices for higher flow rates. However, adding extensional–thickening into the model changes this situation. For both geometries considered here (see Figures 2, 4) we observe clear vortex activity. Moreover, experimentalists have examined the effect of geometry

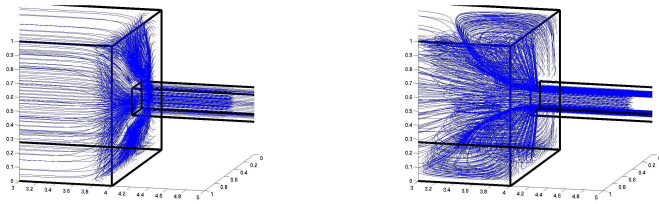

Figure 4: 3D square–to–square contraction geometry. Streamline plots, Newtonian fluid (left figure) and extensional–thickening fluid (right figure).

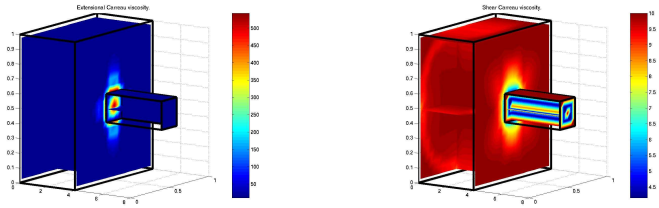

Figure 5: 3D square–to–square contraction geometry. Extensional viscosity (left figure) and shear viscosity (right figure).

on the formation of vortices. The most common test problems considered in the literature are planar and axisymmetric entry flows. For the Newtonian fluids the results show little, or no vortices at the corners for both cases. The observations show, that vortices in planar contraction, if appear, are much smaller than in axisymmetric domain. Similar situation happens in square–to–square geometry, which resembles axisymmetric one. In Figure 2 streamlines plots in 3D planar contraction of the Newtonian (left plot) and the generalized

Newtonian (right plot) fluids, at the same flow rate, are given. For the Newtonian fluid no vortices are noticeable, whereas for the latter one, that exhibits both shear–thinning and extensional–thickening, the vortices are clearly visible. The streamlines plots for the same test fluid in square–to–square geometry is shown in Figure 4. Again, the Newtonian fluids exhibit no vortices, contrary to the generalized Newtonian one. Moreover, the vortices are much larger comparing with 3D planar contraction case, what is in a very good qualitative agreement with experiments. Such behavior is correlated with much higher growth of the extensional stress in 3D square–to–square contraction, what is shown in Figures 3 and 5, where extensional $\eta_e(\dot{\epsilon})$ and shear $\eta(\dot{\gamma})$ viscosities are given. Moreover, for constant $\eta_e(\dot{\epsilon})$, or extensional–thinning fluids no growth of the vortices was detected. Above results may indicate the statement made by White and Kondo in [24], that only materials with clearly strong increasing of the elongational viscosities as a function of extensional rate exhibit vortices.

4.2 Integral models

Let us first present simulation results of dilute polymer solution modeled by integral Oldroyd B model. Numerical computations are performed on regular Cartesian grid in 4:1 2D planar contraction domain. We use the same space grid steps in all coordinates directions. In all simulation, the time step used is $\tau = 5 \cdot 10^{-3}$. The calculations have been performed for a range of Weissenberg numbers, which is defined as $We = \lambda \cdot \frac{\bar{U}}{L}$, where λ is the relaxation time, $\bar{U}$ is the mean outflow velocity and L is the outflow channel width. We perform comparison with the simulations obtained in [1, 2, 3, 16, 20], where equivalent differential Oldroyd B model is used. In this case, we keep Re number constant and the change of the We number is due to the change of the relaxation time λ. To quantify the size of the vortices we use the reattachement length L_v. Let us present quantitative comparison with the results obtained by differential counterpart. We compare our work

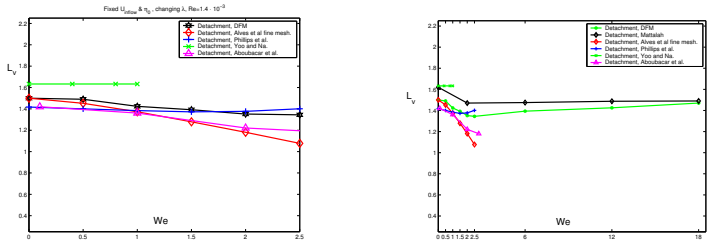

Figure 6: Reattachement lengths against We numbers (left figure). Reattachement lengths against We numbers for high We numbers (right figure).

with the results presented in [1, 2, 3, 16, 20]. To be consistent with those findings we have chosen the following fluid parameters: $\rho = 1[\frac{g}{cm^3}]$, $\eta_s = 1[Pa\ s]$ and $\eta_p = 8[Pa\ s]$. Time discretization of the integral constitutive equation is performed via Deformation Field Method. The simulations are performed for constant $Re = 10^{-3}$. We change We number

by changing relaxation time λ. We observe decrease in the reattachement lengths as We is increased, what is consistent with [1, 2, 3, 16, 20]. Results for the vortex behavior are presented in Figure 6. The left figure shows comparison of the vortex behavior with the previously published values for low Weissenberg numbers. As it was pointed out in [3], there is dispersion in these results, however our findings fall in the range of listed data. In right plot of Figure 6 we show comparison of the reattachement lengths with [16] for high Weissenberg numbers. The reattachement lengths are a bit lower in our simulations, however for $We = 18$ results coincide. We would like to point out, that we have no problems with performing calculation for high We numbers.

Let us now present results obtained form simulations of concentrated polymer solutions. Two nearly monodisperse solutions, with an experimental data available in [6, 11] and [22], are taken into considerations. The extra stress tensor is modeled by the most

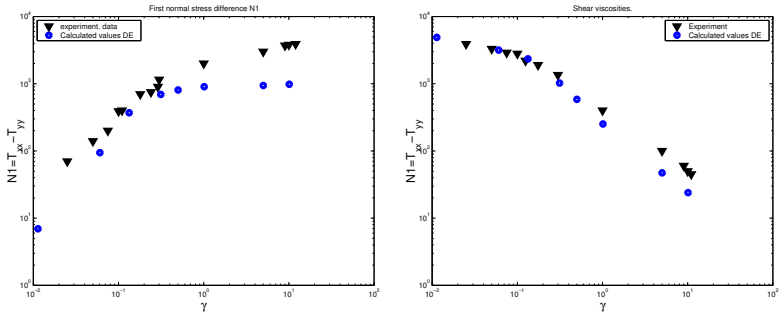

Figure 7: Rheological results for polystyrene solution. Left figure presents comparison of $N_1 = T_{xx} - T_{yy}$ between the experimental data (black triangles) given in [6] and calculated results (blue circle) against shear–rate $\dot{\gamma}$. Right figure presents comparison of the shear viscosity, defined as $\eta(\dot{\gamma_{xy}}) = \frac{T_{xy}}{\dot{\gamma_{xy}}}$, against shear–rate $\dot{\gamma_{xy}}$ between experimental measurements and calculated results.

successful tube model described by the time integral constitutive equation (15) introduced by Doi and Edwards (in 1986). Results are evaluated in rheometrical flow. It is well known, that viscoelastic fluids, contrary to the Newtonian one, exhibit non zero first normal stress difference $N_1 = T_{xx} - T_{yy}$ in steady state–state shear flows. In [6], Bhattacharjee et al. have published experimental data in both shear and extension for a 10% solution of a $3.9 \cdot 10^6$ molecular weight polystyrene in diethyl phthalate. In addition, they have derived the values for the Doi Edwards model parameters, which are: $\rho = 1[\frac{g}{cm^3}]$, $G_e = 3083[Pa]$, $\tau_d = 8.61[s]$ and $\eta_0 = 4570[Pa\ s]$. For a numerical comparison of simulation results and rheological data of the first normal stress difference N_1, as well as the shear viscosity defined as $\eta(\dot{\gamma}_{xy}) = \frac{T_{xy}}{\dot{\gamma}_{xy}}$, we choose the plane Couette flow. Therefore, as a test geometry the channel with upper wall moving at a constant velocity and static lower wall is taken. At the inflow linear velocity profile, known analytically form the Newtonian Couette flows, is imposed. At the outflow zero Neumann condition for velocities is satisfied. Note, that in these comparison equations (3), (4) supplemented by model (15) are solved, and the simulations are performed till the steady state is reached.

For the comparison, similarly as in [6], the modulus G_e is scaled in such a way, that the zero–shear viscosity of the model coincides with the zero–shear viscosity of the data, i.e. $\eta_0 = 4570[Pa\ s]$. In Figure 7 comparison between experimental measurements and the values obtained from the simulations, sampled at the middle point of the channel, and thus being at less influenced by the boundaries, are shown. Left plot shows comparison of the first normal stress difference $N_1 = T_{xx} - T_{yy}$. At regimes, where $\dot{\gamma} < 1$ simulation results show very good agreement with experimental observations. For higher shear–rates regimes, however, the original Doi Edwards model (15) gives lower predictions than experimental values. The same observations are showed in [6, 22], where authors have used differential approximation to the Doi Edwards integral model. Right plot from Figure 7 presents comparison of the shear viscosity sampled experimentally and calculated through the formula $\eta(\dot{\gamma}_{xy}) = \frac{T_{xy}}{\dot{\gamma}_{xy}}$. Again, very good quantitative agreement with experiment is achieved.

4.3 Performance of different solution techniques

Let us finally present results from comparison of the performance of three solution algorithms: SIMPLE–like projection method (where mixed derivatives are treated in explicit way), coupled momentum projection method (where mixed derivatives are treated in implicit way) and fully coupled method, in terms of stability of calculations that could be achieved. For that, the following numerical experiment was performed. An unsteady problem, starting simulations from the liquid being at rest and calculating till reaching the steady state, is solved. Three fluids with different viscosity properties, namely shear–thinning (with fluid parameters $Cu = 1.0$, $n = 0.2$), shear–thinning and extensional–

η_0	1	10	50	100	500	1000	2500	5000	7500
SIMPLE like	Con.	Con.	Div.	Div.	Div.	Div.	Div.	Div.	Div.
Coupled momentum	Con.	Con.	Con.	Con.	Con.	Con.	Con.	Con.	Con.
Fully coupled	Con.	Con.	Con.	Con.	Con.	Con.	Con.	Con.	Con.

Table 1: Stability performance of three different solution techniques for shear–thinning fluid, modeled by the Carreau constitutive equation (6), with the fluid parameters $Cu_s = 1.0$, $n_s = 0.4$.

thickening ($Cu = 1.0$, $n = 0.2$, $Cu_e = 1.0$, $n_e = 0.4$), and finally shear–thickening and extensional–thinning ($Cu = 1.0$, $n = 1.1$, $Cu_e = 1.0$, $n_e = 0.4$), were selected. The simulations were performed in planar 4:1 contraction domain with the time step $\tau = 10^{-3}$. The only parameter that was varied was the zero shear–rate viscosity η_0. In all the cases the flow was such, that the mean velocity in the smaller outflow channel $\bar{U} = 10[\frac{cm}{s}]$ (if the steady state was reached). In Tables 1, 2, 3 the simulations result of the listed

above fluids are presented, where we indicate for which zero shear–rate viscosity η_0 the corresponding solution techniques converged (denoted by Con.) and gave steady state solution, or diverged (denoted by Div.) and no solution was obtained. In all the cases, as expected, the most stable behavior was obtained by the coupled momentum projection method and the fully coupled method. For all range of the zero shear–rate viscosities, that has been taken into considerations, stable steady–state solutions were reached. The

η_0	1	10	50	100	500	1000	2500	5000	7500
SIMPLE like	Con.	Con.	Con.	Con.	Con.	Con.	Con.	Con.	Con.
Coupled momentum	Con.	Con.	Con.	Con.	Con.	Con.	Con.	Con.	Con.
Fully coupled	Con.	Con.	Con.	Con.	Con.	Con.	Con.	Con.	Con.

Table 2: Stability performance of three different solution techniques for shear–thinning and extensional–thickening fluid, modeled by the extension of the Carreau constitutive equation (10), with the fluid parameters $Cu_s = 1.0$, $n_s = 0.4$, $Cu_e = 1.0$, $n_e = 1.1$.

η_0	1	10	50	100	500	1000	2500	5000	7500
SIMPLE like	Con.	Div.	Div.	Div.	Div.	Div.	Div.	Div.	Div.
Coupled momentum	Con.	Con.	Con.	Con.	Con.	Con.	Con.	Con.	Con.
Fully coupled	Con.	Con.	Con.	Con.	Con.	Con.	Con.	Con.	Con.

Table 3: Stability performance of three different solution techniques for shear–thickening and extensional–thinning fluid, modeled by the extension of the Carreau constitutive equation (10), with the fluid parameters $Cu_s = 1.0$, $n_s = 1.1$, $Cu_e = 1.0$, $n_e = 0.4$.

least stable was the SIMPLE–like solution algorithm. As expected, explicit discretization of the mixed derivatives has led to stability problems. The stable simulations could be obtained for all considered η_0 only in the case of the shear–thinning and extensional–thickening fluid. However, for shear–thinning fluid (Table 1), and for shear–thickening and extensional–thinning one (Table 3), stable calculations were obtained up to $\eta_0 = 10$ and $\eta_0 = 1$, respectively. This can be explained from the fact, that for the first fluid the extensional viscosities that enter diagonal blocks of the viscous operator $\eta_e \geq \eta_0$ (since the fluid is extensional–thickening) and the shear viscosities $\eta_s \leq \eta_0$ enter the off–diagonal ones. This results in stronger block diagonal dominance of the viscous operator,

which is not the case for the last two remaining fluids. We have also observed, that for large viscosities ($\eta_0 \geq 5000$) the convergence rate of the projection type methods (if they have converged) was very poor, and high number of the non–linear iterations had to be performed in order to get satisfactory result. It was not the case for the fully coupled method.

5 CONCLUSIONS

In this paper, we have proposed new anisotropic viscosity model being able to deal with shear and extensional properties of viscoelastic fluids. It has shown very good agreement with experimental observations in various contraction flows. Moreover, we have presented simulation results of dilute and concentrated polymer solutions described by integral Oldroyd B and integral Doi Edwards models respectively. Simulations show very good agreement with experimental observations (Doi Edwards model), as well as with the results obtained by differential counterpart (Oldroyd B model). It is also shown here, that careful treatment of mixed derivatives from momentum equations is essential in performing stable simulations of generalized Newtonian fluids.

REFERENCES

[1] M.Aboubacar, H.Matallah, M.F.Webster, *Highly elastic solutions for Oldroyd-B and Phan-Thien/Tanner fluids with a finite volume/element method: planar contraction flows*, *J.Non-Newtonian Fluid Mech.* **103**, pp 65-103 (2002).

[2] M.Aboubacar, T.N.Phillips, H.R.Tamaddon-Jahromi, M.F.Webster, A.J.Williams, *Numerical simulation of contraction flows for Boger fluids using finite volume methods.*

[3] M.A.Alves, P.J,Oliviera, F.T.Pinho, *Benchmark solutions for the flow of Oldroyd-B and PTT fluids in planar contractions*, *J.Non-Newtonian Fluid Mech.* **110**, pp 45-75 (2003).

[4] Axelsson O., Neytcheva M., *Preconditioning methods for linear systems arising in constrained optimization problems*, *Numerical Linear Algebra with Applications***10**,2003,pp 1-26.

[5] Barrett R., Berry M., Chan T.F., Demmel J., Donato J., Dongarra J., Eijkhout V., Pozo R., Romine C., and Van der Vorst H.. *Templates for the Solution of Linear Systems: Building Blocks for Iterative Methods*, SIAM, Philadelphia, PA, 1994.

[6] P.K. Bhattacharjee, D.A. Nguyen, G.H.McKinley, T.Sridhar, *Extensional stress growth and stress relaxation in entangled polymer solutions*, *J. Rheol.*, **47** , 269-290 (2003).

[7] Doi M., Edwards S.F., The Theory of Polymer Dynamics, *Oxford University Press, New York*, 1986.

[8] C.A.J.Fletcher, *Computational Techniques for Fluid Dynamics*, (Springer-Verlag, 1991).

[9] Iliev O., Linn J., Moog M., Niedziela D., Starikovicius V. *On the performance of certain iterative solvers for coupled systems arising in discretization of non-Newtonian flow equations*, *ECCOMAS*, 2004.

[10] Iliev O., Stoyanov D., *Multigrid - adaptive local refinement solver for incompressible flows*, *Berichte des Fraunhofer ITWM*, **54**, 2003

[11] G.Ianniruberto, G.Marrucci, *A multi–mode CCR model for entangled polymers with chain stretch*, *J.Non-Newtonian Fluid Mech.*, **102**, pp. 383-395 (2002).

[12] Kime-E M.E., Brown R.A., Armstrong R.C., *The roles of inertia and shear-thinning in flow of an inelastic liquid through an axisymmetric sudden contraction*, *J. Non-Newtonian Fluid Mech.*, **13**,1983,341-363.

[13] Evans R.E., Walters K., *Flow characteristics associated with abrupt changes in flow geometry in the case of highly elastic liquids*, *J.Non-Newtonian Fluid Mech.* **20**,1986,pp 11-29.

[14] Feigl K., Tanner F.X., Edwards B.J., Collier J.R., *A numerical study of the measurements of elongational viscosity of polymeric fluids in a semihyperbilically converging die*, *J. Non-Newtonian Fluid Mech.*, **115** (2-3),2003,pp 191-215.

[15] M. Gerritsma, *Time dependent Numerical Simulations of a Viscoelastic Fluid on a Staggered Grid*, (1996).

[16] H.Matallah, P.Townsend, M.F.Webster, *Recovery and stress-spliting schemes for viscoelastic flows*, *J.Non-Newtonian Fluid Mech.*, **75**, pp. 139-166 (1998).

[17] Owens R.G., Phillips T.N., *Computational Rheology*, *Imperial College Press*, 2002.

[18] E.A.J.F.Peters, Generalization of the deformation field method to simulate advanced reptation models in complex flows, *J.Rheol.*, **44**, pp 811-829 (2000).

[19] E.A.J.F.Peters, M.A. Hulsen, B.H.A.A van den Brule, *Instationary Eulerian viscoelastic flow simulation using time separable Rilivin-Sawyers constitutive equations*, *J.Non-Newtonian Fluid Mech.* **89** (2000) 209-228.

[20] T.N.Phillips, A.J.Williams, *Viscoelastic flow through a planar contraction using a semi-Lagrangian finite volume method*, *J.Non-Newtonian Fluid Mech.* **87**, pp 215-246 (1999).

[21] Turek S., *Efficient solvers for incompressible flow problems: An algorithmic approach in view of computational aspects*, Springer, 1998/99.

[22] P. Wapperom, R. Keunings, *Impact of Decoupling Approximation Between Stretch and Orientation in Rheometrical and Complex Flow of Entangled Polymers*, *J. Non-Newtonian Fluid Mech.*, **122** , 33-43 (2004).

[23] White S.A., Baird D.G., *The importance of extensional flow properties on planar entry flow patterns of polymer melts J.Non-Newtonian Fluid Mech.* **20**,1986,pp 93-102.

[24] White J.L., Kondo A., *Flow patterns in polyethylene and polystyrene melts during extrusion through a die entry region: measurement and interpretation J.Non-Newtonian Fluid Mech.* **3**,1977,pp 41-64.